NANO LETTERS

Letter

pubs.acs.org/NanoLett

# Biaxial Strain Transfer in Supported Graphene

C. Bousige,[†] F. Balima,[†] D. Machon,[*,†] G. S. Pinheiro,[†,#] A. Torres-Dias,[†] J. Nicolle,[△] D. Kalita,[‡] N. Bendiab,[‡] L. Marty,[‡] V. Bouchiat,[‡] G. Montagnac,[∥] A. G. Souza Filho,[⊥] P. Poncharal,[†] and A. San-Miguel[*,†]

[†]Univ. Lyon, Université Claude Bernard Lyon 1, CNRS, Institut Lumire Matière, F-69622, Villeurbanne, France

[‡]Institut Néel, Université Grenoble Alpes, BP 166, Grenoble Cedex 9, 38042, France

[∥]Univ. Lyon, Université Lyon 1, Laboratoire de Géologie de Lyon, CNRS, Ecole Normale Supérieure de Lyon, 46 allée d'Italie, BP 7000, 69342 Lyon Cedex 07, France

[⊥]Departamento de Física, Universidade Federal do Ceará, Fortaleza, P.O. Box 6030, Ceará 60455-900, Brazil

[#]Departamento de Física, Campus Ministro Petrônio Portella, Universidade Federal do Piauí, Teresina, Piauí 64049-550, Brazil

[△]Laboratoire Interface Confinement Matériaux et Nanostructures, UMR 7374, 1b rue de la Ferrolerie, 45071 Orléans Cedex 2, France

**ABSTRACT:** Understanding the mechanism and limits of strain transfer between supported 2D systems and their substrate is a most needed step toward the development of strain engineering at the nanoscale. This includes applications in straintronics, nanoelectromechanical devices, or new nanocomposites. Here, we have studied the limits of biaxial compressive strain transfer among $SiO_2$, diamond, and sapphire substrates and graphene. Using high pressure—which allows maximizing the adhesion between graphene and the substrate on which it is deposited—we show that the relevant parameter governing the graphene mechanical response is not the applied pressure but rather the strain that is transmitted from the substrate. Under these experimental conditions, we also show the existence of a critical biaxial stress beyond which strain transfer become partial and introduce a parameter, $\alpha$, to characterize strain transfer efficiency. The critical stress and $\alpha$ appear to be dependent on the nature of the substrate. Under ideal biaxial strain transfer conditions, the phonon Raman G-band dependence with strain appears to be linear with a slope of $-60 \pm 3$ cm$^{-1}$/% down to biaxial strains of $-0.9$%. This evolution appears to be general for both biaxial compression and tension for different experimental setups, at least in the biaxial strain range $-0.9\% < \varepsilon < 1.8\%$, thus providing a criterion to validate total biaxial strain transfer hypotheses. These results invite us to cast a new look at mechanical strain experiments on deposited graphene as well as to other 2D layered materials.

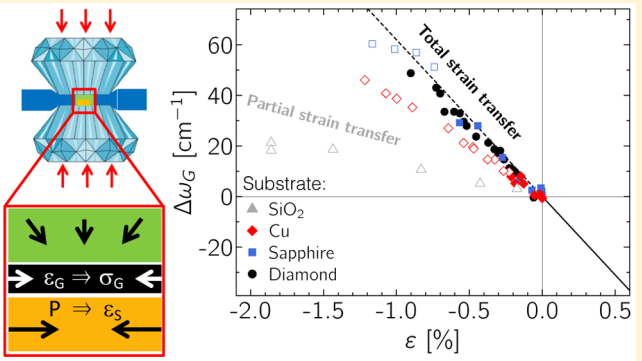


**KEYWORDS:** *Graphene, 2D materials, strain engineering, adhesion, Raman spectroscopy, high pressure*

Since its mechanical isolation by exfoliation,[1−4] graphene has attracted a lot of interest due to an unusual quantum Hall effect,[1,3] its electric[5] and magnetic properties,[6] or its exceptional mechanical properties.[7] Furthermore, the existence of a strong coupling between the mechanical and the electronic properties of graphene[8−10] allows developing bidimensional strain engineering as a route for technological applications of graphene.[11] However, the bidimensional nature of graphene still challenges our understanding of its mechanical response, and a precise determination and monitoring of the stress response of graphene in various conditions has become a key requirement for such developments.[12] A fine description of the mechanical response of graphene to strain conditions when in contact with different interfaces is thus at the cornerstone of the development of devices, graphene-based composites, or in the understanding of the physical processes in tribological graphene-based interfaces.[13] Assessing the general interplay between the mechanics of graphene and adhesion will contribute to the understanding of the response of this archetype bidimensional material to a changing environment and thus to the development of various stress sensors.[14,15] Adhesive forces moreover constitute a key parameter participating in determining the maximum stress that can be transmitted to graphene from the substrate it is deposited on: it has for example been shown that graphene adhesion to polymers in a sandwich geometry provides a dramatic enhancement of its flexural rigidity, the latter being 6 orders of magnitude larger than in air.[16]

**Received:** July 18, 2016
**Revised:** November 29, 2016
**Published:** November 29, 2016





DOI: 10.1021/acs.nanolett.6b02981
*Nano Lett.* XXXX, XXX, XXX−XXX

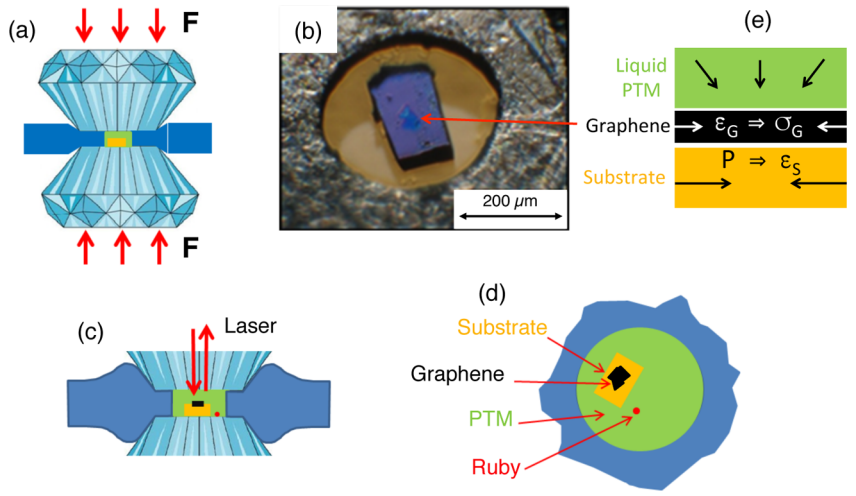


**Figure 1.** (a) Diamond anvil cell principle. The sample is confined in between two diamonds and a hollowed metallic gasket and immersed in the pressure transmitting medium (PTM). The force applied on the diamonds induces the pressure increase through the deformation of the sample chamber: (b) Picture of the sample chamber in which a graphene sample is supported on a thick substrate (the visible part is a multilayered area). (c and d) Two pictorial views (axial and radial) of the loading scheme. The small sphere next to the substrate represents a ruby chip in which fluorescence is used to determine the sample pressure.[33,34] Panel e is a representation of the mechanical constraints in which the graphene sample is found in our experiments. The hydrostatic pressure imposed by the liquid PTM induces a contraction of the substrate (strain $\varepsilon_S$), a deformation that is (partly) transmitted to the graphene layer that is strained as $\varepsilon_G$, which results into a stress $\sigma_G$.

In the majority of experiments or applications, graphene is supported by a substrate. Up to now, most studies on the mechanical response of graphene have been devoted to its tensile response, either under uniaxial[7,12,17] or biaxial tension.[18−21] Large compressive strain values can also be achieved in high-pressure experiments,[22−24] which allow maximizing the coupling between graphene and the supporting substrate—and thus the interfacial strain transfer. The two main assumptions made in most of these studies are that (1) the perfect graphene conformation to its substrate[25] is preserved under strain and (2) that the totality of the substrate deformation is transmitted to the deposited graphene flake. The derivation of many physical parameters such as the Grüneisen parameter relies on these hypotheses.

The latter hypothesis of total strain transfer between the substrate and the graphene flake is a key aspect. This hypothesis has already been tested before in tension experiments, but it was shown not being always true.[19,26,27] It is thus the aim of the present work to *quantify* such strain transfer in the most favorable conditions (i.e., by maximizing the conformation between the substrate and graphene by pressure application) as well as to explore its validity in the biaxial compression domain.

We have studied here by Raman spectroscopy the high-pressure behavior of single-layered graphene samples either exfoliated and supported on amorphous $SiO_2$ substrates or CVD-grown and transferred on diamond and sapphire substrates. In all experiments, the sample was loaded in a diamond anvil cell (DAC), as shown in Figure 1. We show that the relevant parameter governing the graphene behavior is not the applied pressure, but rather the biaxial strain that is transmitted from the substrate, and that this strain is not always fully transmitted from the substrate to the graphene flake. We identify a measurable parameter $\alpha$ characterizing the efficiency of strain transfer and report its evolution with graphene stress for different substrates. These results invite us to cast a new look at experiments considering supported graphene under mechanical strain.

In our experiments, as shown on Figure 1, graphene is supported on substrates with various compressibilities and immersed in a compressive fluid in the experimental chamber of a diamond anvil cell. The DAC allows the compression of the graphene−substrate system up to pressures in the few GPa range. The progressive compression of the fluid on the full system translates into two different effects: (1) the reduction of the graphene−substrate distance with the consequent evolution of adhesion forces and (2) the biaxial compression of graphene due to the volume reduction of the substrate. The only condition for this is that the graphene sample initially immersed is already in an adhesive configuration, which will not allow the PTM to invade the space in between the substrate and the graphene layer. It has been shown that near-perfect graphene−substrate adhesion can be obtained (99% conformation to the surface), from ultraflat graphene on mica substrates[35] to $SiO_2$ substrates with roughness rms of 0.35 nm,[25] and the limits of adhesion of graphene as a function of the surface topology are now well-understood.[36] Anisotropic effects can be neglected in our experiments, as either the substrate is amorphous when graphene is a single crystal ($SiO_2$ case), or graphene is polycrystalline when the substrate is a single or poly crystal (all other cases). In addition, it has been shown that anisotropic effects between armchair and zigzag directions are negligible.[37]

The $SiO_2$ substrate used in the present study is identical to the one in ref 24, with a roughness rms of 0.35 nm. High-resolution atomic force microscopy (AFM) measurements have shown that perfect graphene−substrate conformation is obtained even for structures with radius of curvature of the order of ∼1 nm[25] such as $SiO_2$. High fidelity conformation is thus expected for the sapphire and diamond substrates, for which we measured roughness rms of 0.9 and 0.3 nm, respectively.

The evolution of the 2D band (also called the G′-band) has been proposed as the most sensitive signature of graphene strain.[38] In our high-pressure experiments, its use is hindered by the parasitic Raman signal of the diamond anvil in the corresponding energy range. Thus, we have focused on the


DOI: 10.1021/acs.nanolett.6b02981
Nano Lett. XXXX, XXX, XXX−XXX

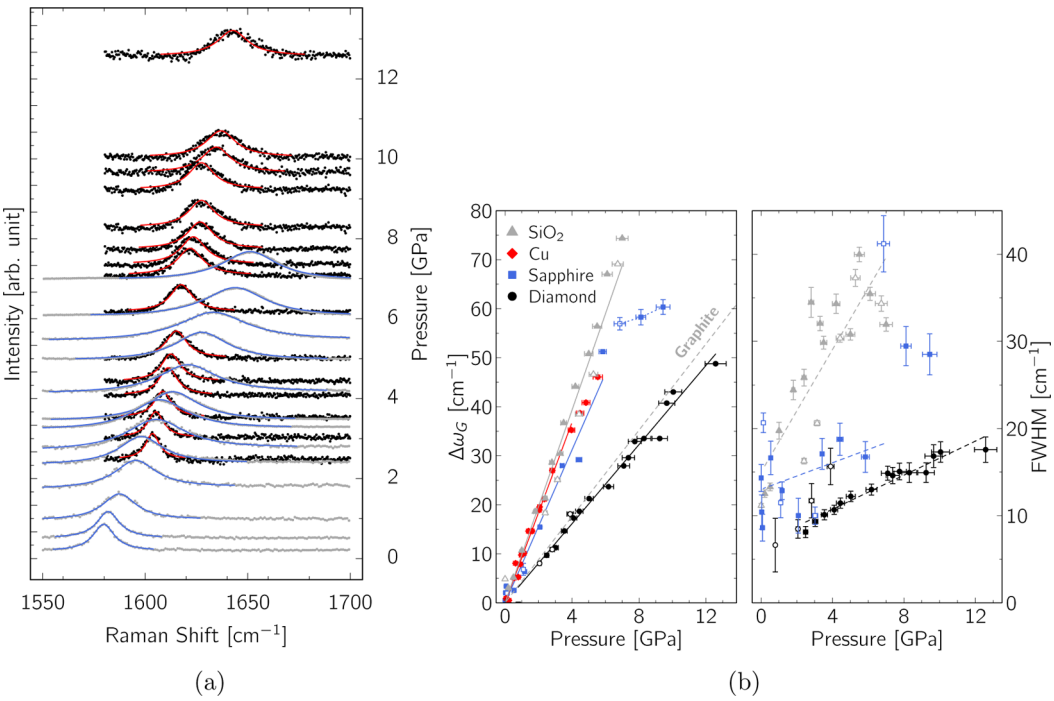


**Figure 2.** (a) Pressure evolution of the Raman spectra (zoom on the G-band only) of graphene deposited on diamond (black points, red line) and $SiO_2$ (gray points, blue line) in alcohol pressure transmitting medium (PTM). The lines are Lorentzian fits, and the spectra baselines correspond to the pressure (right axis). (b) Pressure evolution of the G-band variation (left), $\Delta\omega_G = \omega(P) - \omega_0$ (where $\omega_0$ is the Raman frequency at atmospheric pressure), for graphene deposited on various substrates: black circles correspond to diamond substrate, blue squares to sapphire, gray triangles to $SiO_2$, and red diamonds to copper (the latter being reproduced from ref 23). Open symbols correspond to decreasing pressure. Full lines show linear fits of the G-band variation in the low-pressure range. For comparison, the dashed line recalls the same evolution in the case of graphite.[39] The Lorentzian fwhm are reported in the right panel. Dashed lines are a guide to the eyes. For all data reported in this figure, the 4:1 methanol:ethanol mixture was used as PTM.

**Table 1. Characteristic Parameters Obtained for Graphene on the Four Studied Substrates: Pressure Evolution of the G-Band Frequency $\partial\omega_G/\partial P$, Substrate Linear Bulk Modulus $\beta_S$, Critical Graphene Stress $\sigma_G^c$, and Efficiency of Strain Transmission $\alpha$ above and below the Critical Stress**[a]

| | $\partial\omega_G/\partial P$ (cm$^{-1}$·GPa$^{-1}$) | $\beta_S$ (GPa) | $\sigma_G^c$ (GPa) | $\alpha(\sigma_G)$ for $\sigma_G < \sigma_G^c$ | $\alpha(\sigma_G)$ for $\sigma_G > \sigma_G^c$ |
|---|---|---|---|---|---|
| diamond | 4.0 ± 0.2 | 1329 | >11 | 0.97 ± 0.05 | |
| sapphire | 7.8 ± 0.5 | 750 | 10 ± 1 | 0.97 ± 0.05 | 0.2 ± 0.1 |
| copper[23] | 9.2 ± 0.3 | 420 | 2 ± 1 | 0.97 ± 0.1 | 0.62 ± 0.05 |
| $SiO_2$ | 10.5 ± 0.2 | 114 | <1 | | 0.21 ± 0.05 |

[a]Note that, for $SiO_2$ and diamond substrates, precise values of $\sigma_G^c$ could not be determined.

study of the Raman G-band evolution. In Figure 2a we show the pressure evolution of the optical phonons of the G-band for graphene deposited on diamond and $SiO_2$ substrates. All Raman spectra show the blue-shift of the G-band with pressure application and its reversible red-shift upon pressure release. Under both uniaxial tension or compression,[16] measurements have shown that the doubly degenerated $E_{2g}$ graphene optical mode (G-peak) splits into two components, $G^+$ and $G^-$, named after the carbon nanotube G-band structure.[17] This splitting is not observed during high-pressure experiments under hydrostatic or quasi-hydrostatic conditions on supported graphene,[22−24] where no anisotropic in-plane constraint could lead to the degeneracy lifting.

For the three different studied substrates, the G-peaks are fitted using Lorentzian functions after proper fluorescence background removal using polynomial functions, and Figure 2b shows the relative fitted position of the G-band as a function of the pressure. As already shown in previous works,[22−24] the G-band shows a linear up-shift with pressure before gradually becoming sub-linear, which has been attributed to graphene−substrate unbinding.[23] We only observed the G-band softening at high pressure when graphene is supported on a sapphire substrate. Figure 2b also includes data from CVD graphene on a copper substrate reproduced from ref 23. The slopes $\partial\omega_G/\partial P$ of the pressure evolution of the G-band frequency, fitted in the linear domain of each sample, are reported in Table 1. We should note here that, contrary to what was stated in ref 24, no difference of the $\partial\omega_G/\partial P$ was found between data measured using 4:1 methanol−ethanol PTM and published values using argon PTM. This excludes any charge transfer effect from the PTM, in agreement with other works.[23] During the pressure cycle, the G-band showed reversibility for all samples (open symbols in Figure 2b correspond to pressure unloading). In the case of the $SiO_2$ substrate, we could verify that the very weak D-band was unchanged after the pressure cycle. This result further indicates that the pressure cycle did not introduce noticeable defects or extended graphene tearing. The right panel of Figure 2b shows the pressure evolution of


DOI: 10.1021/acs.nanolett.6b02981
Nano Lett. XXXX, XXX, XXX−XXX

the G-band fwhm. For all samples we observe a monotonous increase of the fwhm with pressure. However, at ∼7 GPa in the case of the sapphire substrate, an important discontinuous jump appears, correlated to a change in the evolution of $\Delta\omega_G$.

Usually, in a high-pressure experiment on a 3D sample studied by Raman spectroscopy, the Raman shift is plotted as a function of pressure. The implicit assumption is that the hydrostatic or quasi-hydrostatic stress is transferred to the sample, which is correct until the appearance of nonhydrostatic stress components. This assumption of equivalence between the applied pressure and graphene stress has also been made in previous studies of graphene under high pressure.[22−24] In contrast, in the case of uniaxial stress experiments by the deformation of a substrate under tension, the basic assumption is that it is the strain that is transmitted.[7,12,17,18] The physical properties of graphene (phonons, bandgap, etc.) are thus either determined as a function of the substrate *strain* or *stress*.[7,12,17,18] It thus appears that the underlying assumptions on the mechanical deformations of 2D materials must be clarified, which eventually boils down to determining how efficiently the strains are transmitted from the substrate to the 2D layer. The goal of the following discussion is thus to provide a methodology for (i) renormalizing pressure-based Raman data to stress−strain quantities for allowing a comparison to other types of measurements and (ii) quantifying the efficiency of strain transfer between graphene and the substrate it is deposited on.

Let us consider the physical effects at the scale of the atomic bonds. While the PTM is liquid and since the substrate is a three-dimensional solid, the substrate stress and the pressure are equivalent. The substrate-mediated biaxial strain is then linked to the applied pressure as $\varepsilon_S = P/\beta_S$, where $\beta_S$ is the substrate linear bulk modulus, $\beta_S = -r\partial P/\partial r$ with $r$ being the interatomic distance. The latter can be approximated as $\beta_S \sim 3\beta_S^{3D}$ with $\beta_S^{3D} = -V\partial P/\partial V$ being the bulk modulus, which arises from equating the pressure variation in bond length $r/r_0$ to the variation in lattice constant $a/a_0$: this is possible since the absolute values of $r_0$ and $a_0$ are never used in the calculation.[22,39−41] This approximation boils down to saying that the relative variation in bond length is the same in all directions, which is rather close to reality.[42] The biaxial strain is then transmitted to the graphene layer with an efficiency $\alpha$ (that we want to quantify), so that $\varepsilon_G = \alpha\varepsilon_S$. The strain of the graphene sheet, $\varepsilon_G$, leads to a shift of the Raman frequency of the G-band $\Delta\omega_G$ associated with a given stress $\sigma_G$. In the case of a perfect reference system, the biaxial stress dependence of the Raman shift is given by $\Delta\omega_G = \sigma_G\Omega_{ref} = P\Omega_{ref}$, where $\Omega_{ref}$ is the pressure dependence of the Raman shift. It follows that, for a given Raman shift, the biaxial stress of the graphene sheet deposited on a substrate S can be retrieved through the expression $\sigma_G^S = \Delta\omega_G^S/\Omega_{ref}$. Biaxial stress and strain for graphene are linked through $\varepsilon_G = \sigma_G/\beta_{ref}$, where $\beta_{ref}$ is the in-plane stiffness constant of graphene in the reference case. The graphene biaxial strain is thus linked to the applied pressure through:

$$\sigma_G = \alpha(\sigma_G)\frac{\beta_{ref}}{\beta_S}P \quad (1)$$

where we have considered that the parameter $\alpha$ may vary with the stress $\sigma_G$. A value $\alpha = 1$ corresponds to total strain transfer, while a value $\alpha = 0$ corresponds to a fully unbound 2D layer from the substrate. Intermediate values should be correlated to the proportion of the 2D layer surface for which strain transfer is partial.

We now have to consider the choice of the reference system. A perfect reference sample is a system for which the pressure in the PTM is equal to the stress in the graphene flake. Ideally, this choice should be as close as possible to our initial experimental configuration: PTM−graphene−substrate stacking. The reference would thus correspond to the top first graphene layer in bulk Bernal graphite, where $\alpha = 1$. Assuming that the top graphene sheet in graphite behaves like the bulk ensemble, we have $\Omega_{ref} = 4.4$ cm$^{-1}$/GPa and $\beta_{ref} = 1250$ GPa.[39] One could also have considered as a reference system the case of $\alpha = 0$, which may correspond to the final unbound configuration at very high pressures. In that case, one would have $\Omega_{ref} = 5.6 \pm 0.3$ cm$^{-1}$/GPa[22,23,43] and $\beta_{ref} = C_G/h$, with $C_G = 350$ N/m as the in-plane stiffness constant of graphene (analogous to the Young's modulus for macroscopic objects) and $h = 0.335$ nm as the thickness of the graphene sheet.[44] As the uncertainties on the $\Omega_{ref}$ and $\beta_{ref}$ values are lower in the $\alpha = 1$ case (graphite), we take the graphite system as the reference. We may note that the results that will follow are weakly affected by this choice. Substrate−graphene hybridization may also evolve with pressure application, thus giving rise to a further contribution to the Raman shift. We have neglected such an effect, which will be validated by comparison of our final results with literature, as will be later discussed.

Figure 3a reports the relative evolution of the strains $\varepsilon$ in graphene (G) and in the substrate (S) as a function of the graphene stress $\sigma_G$—the strains being obtained through the equations of state of the corresponding materials. This representation allows identifying the different regimes of strain transfer for each substrate. Figure 3b shows the evolution of $\sigma_G$ as a function of $P \times \beta_{ref}/\beta_S$. From eq 1 we can extract the efficiency coefficient $\alpha$ for the four substrates, whose values are reported in Table 1. Figure 3a shows that two of the substrates, copper and sapphire, present a clear change of regime at values $\sigma_G^c \simeq 2$ and 10 GPa, respectively. For sapphire and copper (for $\sigma_G < \sigma_G^c$) and for diamond, that is, all CVD-grown samples, the same value $\alpha = 0.97 \pm 0.05$ is found within error bars. In the case of $SiO_2$ (the only exfoliated graphene sample), a much smaller value of $\alpha = 0.2 \pm 0.1$ is found. The evolution of $\alpha$ values with $\sigma_G$ is depicted in Figure 4a for the different substrates. It may appear surprising that, in spite of the high graphene conformation to the substrates surfaces, low values of strain transfer can occur, particularly for $SiO_2$. This result highlights the fact that a good conformation of graphene to its substrate does not imply its good adhesion under biaxial strain.

We may now compare our obtained results on the Raman G-band evolution with substrate strain with published results. Biaxial extension and compression has been studied on graphene supported samples on PMMA through piezoactuation[18] or flexion.[19] Helium gas pressure application on suspended graphene has also been used to produce high biaxial tension strain (up to 1.8%).[21] These results are compared with ours in Figure 4b. We observe an excellent agreement between the four very different experimental methods—taking the data for diamond, sapphire, and copper before $\sigma_G^c$ in the case of high pressure experiments where $\alpha = 0.97 \pm 0.05$. This confirms our previously stated hypothesis on the negligibility of pressure-induced hybridization effects. The fit of high-pressure data with $\alpha = 0.9$ yields a slope of $-57 \pm 2$ cm$^{-1}$/% for biaxial compression, which compares very well to the fitted values of $-62 \pm 3$ cm$^{-1}$/% from ref 21, $-57.3 \pm 0.2$ cm$^{-1}$/% from ref 18,


DOI: 10.1021/acs.nanolett.6b02981
Nano Lett. XXXX, XXX, XXX−XXX

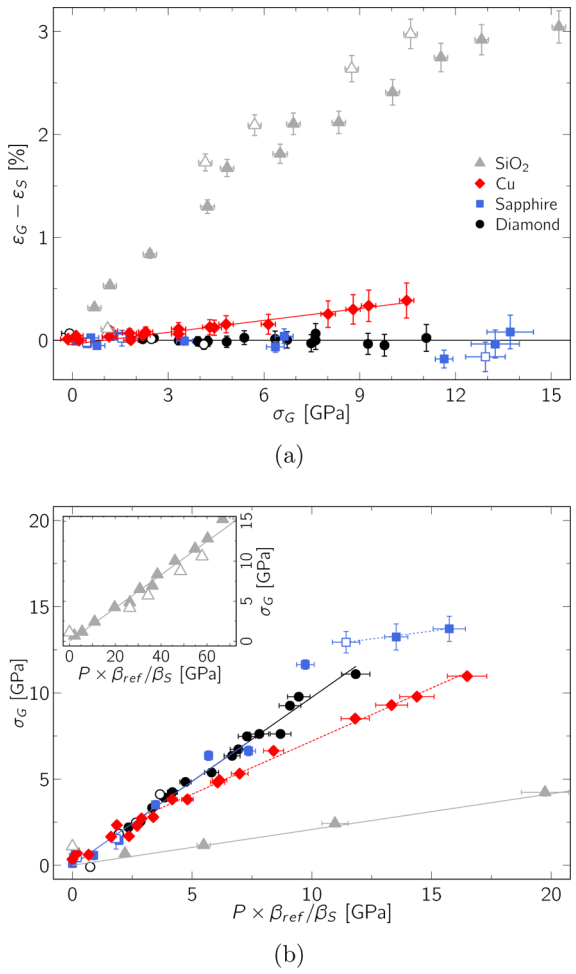


**Figure 3.** (a) Evolution of the graphene strain, $\varepsilon_G$, relative to the substrate one, $\varepsilon_S$, as a function of the graphene stress $\sigma_G$. At the critical stress $\sigma_G^c$, $\varepsilon_G < \varepsilon_S$ (in the case of compression, $\varepsilon < 0$), and slippage occurs (Table 1), corresponding to $\varepsilon_G - \varepsilon_S > 0$. Lines are a guide to the eyes. (b) Graphene stress $\sigma_G$ as a function of $P \times \beta_{ref}/\beta_S$ (eq 1). The slope is directly the efficiency coefficient $\alpha$, obtained by linear fitting (lines and Table 1). The inset shows the total strain range for the $SiO_2$ substrate.

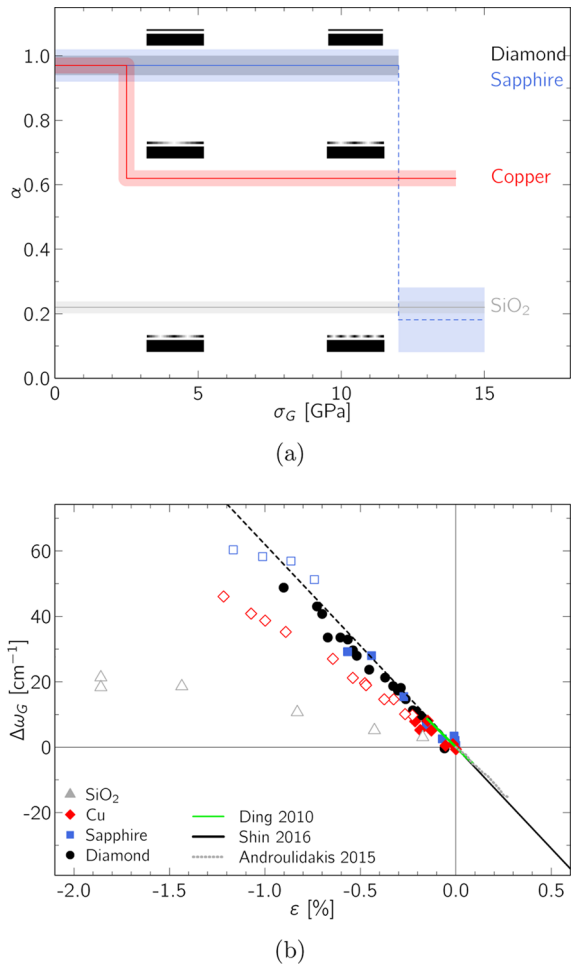


**Figure 4.** (a) Evolution of the biaxial strain transmission efficiency coefficient $\alpha$ as a function of the graphene stress $\sigma_G$. A lower $\alpha$ value implies a larger inhomogeneity in the stress field, as represented in the insets. (b) Evolution of the Raman shift of the G band as a function of the substrate deformation in our DAC experiments, compared with other biaxial strain experiments from refs 18, 19, and 21. Open symbols correspond to $\alpha$ values below 0.97.

or $-62 \pm 5$ cm$^{-1}$/% from ref 19. Such a value thus constitutes a criterion to check for the efficiency of biaxial strain transfer in supported graphene in a large strain range (positive and negative). As shown in Figure 4b, $\alpha$ values below 0.9 (open symbols) lie under the dotted line which is the prolongation of suspended graphene data from ref 21. We observe that, in some cases, close to perfect strain transfer can be preserved down to biaxial strain values of −0.9%. Together with the data of ref 21, our results allow to extend the domain of verified graphene biaxial strain from $\varepsilon = -0.9\%$ up to $\varepsilon = 1.8\%$.

The existence of a partial substrate−graphene strain transfer ($\alpha < 1$) means that an interfacial relaxation mechanism must enter into play. This mechanism could include slipping processes, buckling, defect creation in the graphene structure, or even tearing. The observed reversibility of the Raman signal after a pressure cycle (G and D bands) indicates that defect formation or graphene tearing should not contribute significantly to the relaxation process. A slipping mechanism can either be global, with a full displacement of the graphene flake on the substrate, or local, through the creation of an inhomogeneous stress field. The global case translates into slipping at the micrometer scale through a surface with a nanometer scale roughness: a mechanism which can be excluded at gigapascal pressures. The local case implies the creation of an inhomogeneous strain field (consistent with the G-band fwhm increase with pressure), which should resolve with increasing constraints into the creation of ripples, and ultimately into total unbinding.[45,46]

The difference found between the values of $\sigma_G^c$ for copper and sapphire may be attributed to different surface roughness and adhesion forces in these two cases. We note that for the sapphire substrate, for $\sigma_G > \sigma_G^c$, the fwhm and $\alpha$ values become close to the ones for $SiO_2$ substrate. This may be interpreted as a change in the dominant relaxation mechanism under biaxial strain in sapphire for $\sigma_G > \sigma_G^c$, leading to a partial unbinding of graphene from its substrate. The particularities of the graphene response on copper may arise also from the fact that it is the only substrate on which graphene has been directly grown (no transfer). All observed evolutions in our experiments seem reversible along the pressure cycle, which would exclude a total unbinding process.

The obtained results are extremely important as they fix the limits of validity of the total strain transfer between the


DOI: 10.1021/acs.nanolett.6b02981
Nano Lett. XXXX, XXX, XXX−XXX

substrate and the graphene layer; they invite to cast a new look at mechanical strain experiments on deposited graphene as well as to other 2D layered materials. For instance, the general assumption of total strain transmission in high pressure experiments should be carefully evaluated, and most specifically in the case of substrates such as $SiO_2$. In all type of experiments, a perfect biaxial strain transfer should result in a value of $\partial\Delta\omega_G/\partial\varepsilon = -60 \pm 3$ cm$^{-1}$/%, while for partial strain transfer the absolute value of this slope will decrease. In the latter case, the strain transfer efficiency $\alpha$ becomes smaller than 1. Many other interesting questions arise such as the role of the percolation of the locally strained regions which should form progressively in the $\alpha < 1$ regime, the role of the topology of the locally strained/rippled regions, their development mechanism, or their relation with the substrate roughness or the graphene microstructure (grain size, boundaries, etc.). At ambient conditions the correlation between surface roughness and the buckling transitions has been theoretically shown[45] in a model in which the flexural energies governed by the layer bending rigidity are compared with the geometrical curvature imposed by the surface. We may expect that the extension of such model in high pressure conditions will answer part of these questions.

**Methods.** *Samples.* Exfoliated graphene was used with the $SiO_2$ following similar protocol as in ref 24. $SiO_2$ substrates are 300 nm thick amorphous oxidation layers deposited on 50 $\mu$m thick silicon wafers. The substrates are cleaved in an alcohol bath using a tip in order to obtain a wafer with a typical edge size of 200 $\mu$m. Raman spectra were performed before and after the cleavage in order to check whether the graphene samples are modified by the exposure to alcohol or by the cutting process.

Transfer of CVD-grown graphene was used for the diamond and sapphire substrates. In the diamond case, the transfer was done directly on one of the (1 0 0) oriented diamond anvils of the diamond anvil cell. Sapphire A-plane (1 1 −2 0) oriented substrates of 50 $\mu$m thickness were used. Graphene was grown by CVD on copper foil (25 $\mu$m).[28] The transfer process[29] involves first spin-coating PMMA onto graphene on copper, followed by etching copper in an ammonium persulfate solution (1 g per 100 mL of water). The resulting PMMA/graphene film was transferred directly onto the diamond and sapphire substrates. Acetone was used to remove PMMA, and no annealing was performed on these samples prior to measurement.

*High Pressure.* The high-pressure experiments were carried out using membrane diamond anvil cells with low fluorescence diamonds having a culet size of 700 $\mu$m (Figure 1). A 400 $\mu$m hole drilled in a 100 $\mu$m preindented gasket served as compression chamber. Several ruby chips were distributed throughout the sample chamber, and the pressure was determined using the ruby fluorescence method.[30,31] A 4:1 methanol−ethanol mixture was used as a pressure transmitting medium as it is hydrostatic up to pressures of about 10 GPa, where it solidifies.[32] As the pressure range explored in our experiments is confined below 10 GPa, the measurements are always performed in hydrostatic conditions.

*Raman Scattering Measurements.* Raman spectra were measured in backscattering geometry on two different Raman spectrometers. The first one is a Jobin Yvon Labram HR800 spectrometer, with a spectral resolution of about 0.5 cm$^{-1}$. Spectra were excited using 532 nm radiation from a solid state laser. The beam was focused onto the sample using a long working distance Mitutoyo ×50 or ×80 objective, and the size of the laser probe was ∼2.5 $\mu$m at focus. The second one is an Acton Spectrapro 300i spectrometer, with a spatial resolution of about 0.8 cm$^{-1}$. Spectra were excited using 514.5 nm radiation Ar+ ion gas laser, and the beam was focused using a long working distance Mituyoto ×50 objective. In all cases, the casual heating of the sample by the laser was checked by recording spectra at different incident powers. A power of 3 mW at the entrance of the DAC was found to be convenient for the present study as no red shift for the G-band has been observed—it is estimated that the laser power reaching the sample is ∼5 times lower than the laser power entering the DAC.

## AUTHOR INFORMATION


### Corresponding Authors

*E-mail: denis.machon@univ-lyon1.fr.
*E-mail: alfonso.san-miguel@univ-lyon1.fr.

### ORCID

C. Bousige: 0000-0002-0490-2277


### Notes

The authors declare no competing financial interest.

## ACKNOWLEDGMENTS

C.B., F.B., D.M., A.T.D., J.N., D.K., N.B., L.M., V.B., P.P., and A.S.M. acknowledge financial support by ANR program P2N under Contract ANR-11-NANO-025TRI-CO. C.B. acknowledges support from the PALSE program of the University of Lyon. C.B., D.M. and A.S.M. acknowledge support from the iMUST LABEX program MUSCAT-2D. G.S.P. and A.G.S.F. acknowledge support from CNPq (Brazil), INCT Nano-BioSimes and SisNano. N.B., L.M., and V.B. acknowledge support from EC Graphene Flagship (project no. 604391). The Raman facility in Laboratoire de Géologie de Lyon is supported by the Institut National des Sciences de l'Univers (INSU).

## REFERENCES


(1) Novoselov, K.; Geim, A.; Morozov, S.; Jiang, D.; Zhang, Y.; Dubonos, S.; Grigorieva, I.; Firsov, A. *Science* **2004**, *306*, 666−669.
(2) Novoselov, K.; Geim, A.; Morozov, S.; Jiang, D.; Katsnelson, M.; Grigorieva, I.; Dubonos, S.; Firsov, A. *Nature* **2005**, *438*, 197−200.
(3) Zhang, Y.; Tan, Y.; Stormer, H.; Kim, P. *Nature* **2005**, *438*, 201−204.
(4) Meyer, J.; Geim, A.; Katsnelson, M.; Novoselov, K.; Booth, T.; Roth, S. *Nature* **2007**, *446*, 60−63.
(5) Novoselov, K.; Jiang, Z.; Zhang, Y.; Morozov, S.; Stormer, H.; Zeitler, U.; Maan, J.; Boebinger, G.; Kim, P.; Geim, A. *Science* **2007**, *315*, 1379−1379.
(6) Kim, W. Y.; Kim, K. S. *Nat. Nanotechnol.* **2008**, *3*, 408−412.
(7) Lee, C.; Wei, X.; Kysar, J.; Hone, J. *Science* **2008**, *321*, 385−388.
(8) Ni, Z. H.; Yu, T.; Lu, Y. H.; Wang, Y. Y.; Feng, Y. P.; Shen, Z. X. *ACS Nano* **2008**, *2*, 2301−2305.
(9) Cocco, G.; Cadelano, E.; Colombo, L. *Phys. Rev. B: Condens. Matter Mater. Phys.* **2010**, *81*, 10017.
(10) Huang, M.; Pascal, T.; Kim, H.; Goddard, W.; Greer, J. *Nano Lett.* **2011**, *11*, 1241−1246.
(11) Jing, Z.; Guang-Yu, Z.; Dong-Xia, S. *Chinese Phys. B* **2013**, *22*, 057701.
(12) Huang, M.; Yan, H.; Chen, C.; Song, D.; Heinz, T. F.; Hone, J. *Proc. Natl. Acad. Sci. U. S. A.* **2009**, *106*, 7304−7308.
(13) Berman, D.; Deshmukh, S. A.; Sankaranarayanan, S. K. R. S.; Erdemir, A.; Sumant, A. V. *Science* **2015**, *348*, 1118−1122.




DOI: 10.1021/acs.nanolett.6b02981
*Nano Lett.* XXXX, XXX, XXX−XXX

(14) Frank, O.; Tsoukleri, G.; Riaz, I.; Papagelis, K.; Parthenios, J.; Ferrari, A. C.; Geim, A. K.; Novoselov, K. S.; Galiotis, C. *Nat. Commun.* **2011**, *2*, 255.
(15) Arsat, R.; Breedon, M.; Shafiei, M.; Spizziri, P.; Gilje, S.; Kaner, R.; Kalantar-Zadeh, K.; Wlodarski, W. *Chem. Phys. Lett.* **2009**, *467*, 344−347.
(16) Frank, O.; Tsoukleri, G.; Parthenios, J.; Papagelis, K.; Riaz, I.; Jalil, R.; Novoselov, K. S.; Galiotis, C. *ACS Nano* **2010**, *4*, 3131−3138.
(17) Mohiuddin, T. M. G.; Lombardo, A.; Nair, R. R.; Bonetti, A.; Savini, G.; Jalil, R.; Bonini, N.; Basko, D. M.; Galiotis, C.; Marzari, N.; Novoselov, K.; Geim, A. K.; Ferrari, A. C. *Phys. Rev. B: Condens. Matter Mater. Phys.* **2009**, *79*, 205433.
(18) Ding, F.; Ji, H.; Chen, Y.; Herklotz, A.; Dörr, K.; Mei, Y.; Rastelli, A.; Schmidt, O. G. *Nano Lett.* **2010**, *10*, 3453−3458.
(19) Androulidakis, C.; Koukaras, E. N.; Parthenios, J.; Kalosakas, G.; Papagelis, K.; Galiotis, C. *Sci. Rep.* **2015**, *5*, 18219.
(20) Zabel, J.; Nair, R. R.; Ott, A.; Georgiou, T.; Geim, A. K.; Novoselov, K. S.; Casiraghi, C. *Nano Lett.* **2012**, *12*, 617−621.
(21) Shin, Y.; Lozada Hidalgo, M.; Sambricio Garcia, J.; Grigorieva, I.; Geim, A.; Casiraghi, C. *Appl. Phys. Lett.* **2016**, *108*, 221907.
(22) Proctor, J. E.; Gregoryanz, E.; Novoselov, K. S.; Lotya, M.; Coleman, J. N.; Halsall, M. P. *Phys. Rev. B: Condens. Matter Mater. Phys.* **2009**, *80*, 073408.
(23) Filintoglou, K.; Papadopoulos, N.; Arvanitidis, J.; Christofilos, D.; Frank, O.; Kalbac, M.; Parthenios, J.; Kalosakas, G.; Galiotis, C.; Papagelis, K. *Phys. Rev. B: Condens. Matter Mater. Phys.* **2013**, *88*, 045418.
(24) Nicolle, J.; Machon, D.; Poncharal, P.; Pierre-Louis, O.; San-Miguel, A. *Nano Lett.* **2011**, *11*, 3564−3568.
(25) Cullen, W.; Yamamoto, M.; Burson, K.; Chen, J.; Jang, C.; Li, L.; Fuhrer, M.; Williams, E. *Phys. Rev. Lett.* **2010**, *105*, 215504.
(26) Li, Z.; Kinloch, I. A.; Young, R. J.; Novoselov, K. S.; Anagnostopoulos, G.; Parthenios, J.; Galiotis, C.; Papagelis, K.; Lu, C.-Y.; Britnell, L. *ACS Nano* **2015**, *9*, 3917−3925.
(27) Anagnostopoulos, G.; Androulidakis, C.; Koukaras, E. N.; Tsoukleri, G.; Polyzos, I.; Parthenios, J.; Papagelis, K.; Galiotis, C. *ACS Appl. Mater. Interfaces* **2015**, *7*, 4216−23.
(28) Han, Z.; Kimouche, A.; Kalita, D.; Allain, A.; Arjmandi-Tash, H.; Reserbat-Plantey, A.; Marty, L.; Pairis, S.; Reita, V.; Bendiab, N.; Coraux, J.; Bouchiat, V. *Adv. Funct. Mater.* **2014**, *24*, 964−970.
(29) Li, X.; Cai, W.; An, J.; Kim, S.; Nah, J.; Yang, D.; Piner, R.; Velamakanni, A.; Jung, I.; Tutuc, E.; Banerjee, S. K.; Colombo, L.; Ruoff, R. S. *Science* **2009**, *324*, 1312−1314.
(30) Piermarini, G.; Block, S.; Barnett, J.; Forman, R. *J. Appl. Phys.* **1975**, *46*, 2774−2780.
(31) Mao, H.; Xu, J.; Bell, P. J. *J. Geophys. Res.* **1986**, *91*, 4673−4676.
(32) Klotz, S.; Chervin, J.; Munsch, P.; Le Marchand, G. *J. Phys. D: Appl. Phys.* **2009**, *42*, 075413.
(33) Jayaraman, A. *Rev. Mod. Phys.* **1983**, *55*, 65−108.
(34) Chijioke, A. D.; Nellis, W.; Soldatov, A.; Silvera, I. F. *J. Appl. Phys.* **2005**, *98*, 114905.
(35) Lui, C. H.; Liu, L.; Mak, K. F.; Flynn, G. W.; Heinz, T. F. *Nature* **2009**, *462*, 339−341.
(36) Yamamoto, M.; Pierre-Louis, O.; Huang, J.; Fuhrer, M. S.; Einstein, T. L.; Cullen, W. G. *Phys. Rev. X* **2012**, *2*, 041018.
(37) Zhao, H.; Min, K.; Aluru, N. *Nano Lett.* **2009**, *9*, 3012−3015.
(38) Tsoukleri, G.; Parthenios, J.; Papagelis, K.; Jalil, R.; Ferrari, A. C.; Geim, A. K.; Novoselov, K. S.; Galiotis, C. *Small* **2009**, *5*, 2397−402.
(39) Hanfland, M.; Beister, H.; Syassen, K. *Phys. Rev. B: Condens. Matter Mater. Phys.* **1989**, *39*, 12598.
(40) Mohiuddin, T. M. G.; Lombardo, A.; Nair, R. R.; Bonetti, A.; Savini, G.; Jalil, R.; Bonini, N.; Basko, D. M.; Galiotis, C.; Marzari, N.; Novoselov, K. S.; Geim, A. K.; Ferrari, A. C. *Phys. Rev. B: Condens. Matter Mater. Phys.* **2009**, *79*, 205433.
(41) Zallen, R. *Phys. Rev. B* **1974**, *9*, 4485−4496.
(42) San-Miguel, A.; Polian, A.; Gauthier, M.; Itié, J. P. *Phys. Rev. B: Condens. Matter Mater. Phys.* **1993**, *48*, 8683−8693.
(43) Soldatov, A. V.; You, S.; Mases, M.; Novoselov, K. S. *Graphene 2012*, Abstract Book of the Conference, Brussels, Belgium, 2012.
(44) Lambin, P. *Appl. Sci.* **2014**, *4*, 282−304.
(45) Pierre-Louis, O. *Phys. Rev. E* **2008**, *78*, 021603.
(46) Aitken, Z. H.; Huang, R. *J. Appl. Phys.* **2010**, *107*, 123531.


DOI: 10.1021/acs.nanolett.6b02981
*Nano Lett.* XXXX, XXX, XXX−XXX